Analyzing Bipolar Carrier Transport Characteristics of Diarylamino-Substituted Heterocyclic Compounds in Organic Light-Emitting Diodes by Probing Electroluminescence Spectra

Kyung Soo Son,[†] Masayuki Yahiro,[†] Toshiro Imai,[‡] Hiroki Yoshizaki,[§] and Chihaya Adachi*,[†]

Center for Future Chemistry, Kyushu University, 744 Motooka, Fukuoka 819-0395, Japan, Chitose Institute of Science and Technology, 758-65 Bibi, Chitose, Hokkaido 066-8655, Japan, and Koei Chemical Co., 3-7-2, Nihonbashi-honcho, Chuo, Tokyo 103-0023, Japan

Received February 20, 2008. Revised Manuscript Received May 2, 2008

We analyzed bipolar carrier transport characteristics of diarylamino-substituted heterocyclic compounds (DAHCs) having benzene, pyridine, pyrimidine, or triazine electron-accepting core units and carbazole or β-naphthylamine as electron-donating substituents. The highest occupied molecular and lowest unoccupied molecular orbital levels, carrier injection, and transport characteristics were systematically controlled by changing combinations of the core and substituent units. By analyzing electroluminescence spectra as a probe in four kinds of organic light emitting diode (OLED) structures, we found that the carrier transport characteristics of DAHCs significantly change depending on device structure. We concluded that all DAHCs have bipolar carrier transport characteristics, that is, DAHCs intrinsically possess both hole and electron mobilities that are based on unique molecular structures having both electron-donating and -accepting units. We also demonstrated that carrier injection barriers between DAHCs and adjacent carrier transport layers virtually control the appearance of bipolar characteristics in OLEDs.

I. Introduction

Organic light emitting diodes (OLEDs) have attracted considerable attention because of their high electroluminescence (EL) efficiency and their potential for applications used with flat-panel displays.[1,2] With extensive OLED development, there has been significant progress not only in developing organic semiconductor materials,[3–9] OLED device structures,[10–12] and device fabrication techniques[13–16] but also in understanding organic semiconductor behavior. Understanding such behavior leads to significant improvements of OLED characteristics, such as EL quantum efficiency, energy conversion efficiency, and device stability. To understand carrier transport and injection characteristics of organic semiconductors, in particular, time-of-flight (TOF)[17] and ultraviolet photoelectron spectroscopy (UPS),[18,19] various techniques have been widely used. However, these techniques do not necessarily improve understanding of practical OLED characteristics, such as the hole and electron current ratio and the position of the carrier recombination region. The reason for this is voltage distribution inside multilayer device structures is fairly complicated, and estimating this distribution under double carrier injection conditions is difficult.

Such complicated carrier injection and transport behaviors have been previously reported on 4,4′-*N*,*N*′-dicarbazole-biphenyl (CBP)-based electrophosphorescence devices.[20] In the device structure of indium tin oxide (ITO)/4,4′-bis(*N*-(1-naphthyl)-*N*-phenyl-amino)biphenyl (α-NPD)/CBP doped with *fac*-tris(2-phenylpyridine)iridium ($Ir(ppy)_3$)/2,9-dimethyl-4,7-dipheny-10-phenanthroline (BCP)/tris(8-quinolinolato)aluminum (Alq_3)/MgAg, the CBP layer mainly transported

[†] Kyushu University.
[‡] Chitose Institute of Science and Technology.
[§] Koei Chemical Co.

(1) Burroughes, J. H.; Bradley, D. D. C.; Brown, A. R.; Marks, R. N.; Mackay, K.; Friend, R. H.; Burns, P. L.; Holmes, A. B. *Nature (London)* **1990**, *347*, 539.
(2) Braun, D.; and Heeger, A. J. *Appl. Phys. Lett.* **1991**, *58*, 1982.
(3) Adachi, C.; Tsutsui, T.; and Saito, S. *Appl. Phys. Lett.* **1989**, *55*, 1489.
(4) Kuwabara, Y.; Ogawa, H.; Inada, H.; Noma, N.; Shirota, Y. *Adv. Mater.* **1994**, *6*, 677.
(5) Adachi, C.; Tsutsui, T.; Saito, S. *Appl. Phys. Lett.* **1990**, *56*, 799.
(6) Hamada, Y.; Adachi, C.; Tsutsui, T.; Saito, S. *Jpn. J. Appl. Phys.* **1992**, *31*, 1812.
(7) Bettenhausen, J.; Strohriegl, P.; Brutting, W.; Tokuhisa, H.; Tsutsui, T. *J. Appl. Phys.* **1997**, *82*, 4957.
(8) Hamada, Y.; Sano, T.; Fujita, M.; Fujii, T.; Nishio, Y.; Shibata, K. *Chem. Lett.* **1993**, *22*, 905.
(9) Nakamura, N.; Wakabayashi, S.; Miyairi, K.; Fujii, T. *Chem. Lett.* **1994**, *23*, 1741.
(10) Pfeiffer, M.; Leo, K.; Zhou, X.; Huang, J. S.; Hofmann, M.; Werner, A.; Blochwiz, J. *Org. Electron.* **2003**, *4*, 89.
(11) Gross, M.; Muller, D. C.; Nothofer, H. G.; Scherf, V.; Neher, D.; Brauchle, C.; Meerholz, K. *Nature* **2000**, *405*, 661.
(12) Baldo, M. A.; Obrien, D. F.; You, Y.; Shoustikov, A. *Nature* **1998**, *395*, 151.
(13) Schmitz, C.; Thelakkat, M.; Schmidt, H. W. *Adv. Mater.* **1999**, *11*, 821.
(14) Schmitz, C.; Posch, P.; Thelakkat, M.; Schmidt, H. W. *Phys. Chem. Chem. Phys.* **1997**, *1*, 1777.
(15) Schmitz, C.; Schmidt, H. W.; Thelakkat, M. *Chem. Mater.* **2000**, *12*, 3012.
(16) Zou, L.; Savvateev, V.; Booher, J.; Kim, C. H.; Shinar, J. *Appl. Phys. Lett.* **2001**, *79*, 2282.
(17) Pope M.; Swenberg, C. E. *Electronic Process in Organic Crystal*; Clarendon Press: Oxford, 1982.
(18) Sugiyama, K.; Yoshimura, D.; Ito, E.; Miyazaki, T.; Hamatani, Y.; Kawamoto, I.; Ishii, H.; Ouchi, Y.; Seki, K. *Synth. Met.* **1997**, *86*, 2425.
(19) Ishii, H.; Sugiyama, K.; Ito, E.; Seki, K. *Adv. Mater.* **1999**, *11*, 605.
(20) Adachi, C.; Kwong, R. C.; Forrest, S. R. *Org. Electron.* **2001**, *2*, 37.

10.1021/cm8004985 CCC: $40.75
Published on Web 06/14/2008

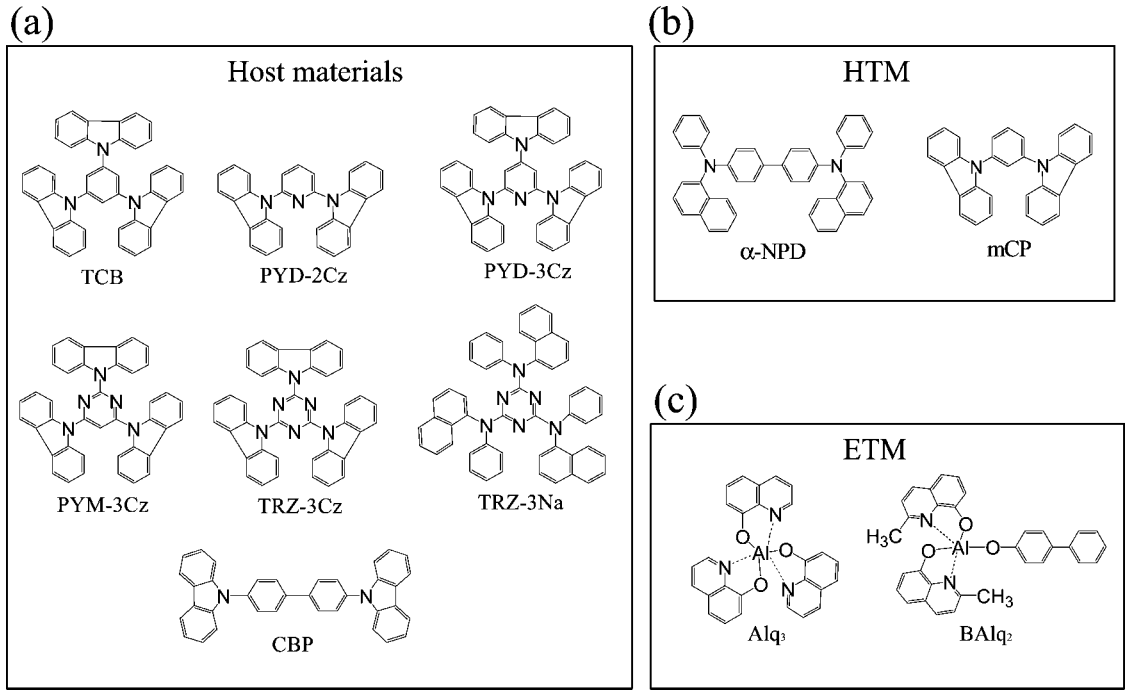

Figure 1. Chemical structures of (a) host materials, (b) hole transport materials (HTM), and (c) electron transport materials (ETM) used in this study.

holes rather than electrons. On the other hand, for ITO/4,4′,4″-tris(3-methylphenylphenyl amino)triphenylamine (m-MTDATA)/CBP doped with $Ir(ppy)_3$/MgAg, the CBP layer mainly transported electrons. These results show that carrier transport characteristics significantly change depending on device structures and their material composites. Similar changes, which depend on device structures, were also reported in 9,10-bisstyrylanthrance derivatives.[21]

Useful for host materials in electrophosphorescence OLEDs, well-balanced bipolar characteristics with high triplet energy levels are needed to obtain high EL efficiency. Although CBP has widely been used as a host material in electrophosphorescence OLEDs,[22,23] its triplet energy level is not satisfactory for pure blue emission,[24] and the hole-transport mobility, which is significantly higher than the electron mobility, sometimes leads to an unbalanced hole and electron recombination. Thus, to obtain more efficient OLED performance, novel host materials providing well-balanced carrier injection and transport ability have been needed.

Aiming for bipolar host materials in our previous study, we synthesized triazine (TRZ) derivatives and used them as a host material in green electrophosphorescence OLEDs.[25] In particular, we demonstrated high EL quantum efficiency using 2,4,6-tricarbazolo-1,3,5-triazine (TRZ-3Cz) having three carbazole substituents, leading to a high external EL quantum efficiency of $\eta_{ext} \sim 10\%$.[25] This is the result of a significantly high triplet energy level ($E_T = 2.81$ eV) of TRZ-3Cz, which is higher than $E_T = 2.56$ eV of the standard CBP. Such high triplet energy characteristics were also identified by theoretical calculation of TRZ derivatives by Chu et al.[26] Although the TRZ derivatives are an excellent host material in electrophosphorescence OLEDs, their carrier injection and transport characteristics are not well understood. Recently, we further synthesized 2,6-dicarbazolo-1,5-pyridine (PYD-2Cz) ($T_1 = 2.93$ eV) and 2,4,6-tricarbazolo-1,3,5-pyrimidine (PYM-3Cz) ($T_1 = 2.84$ eV), which have higher triplet energy levels, and demonstrated that these host materials are useful for blue electrophosphorescence OLEDs.[27,28]

In this study, we systematically prepared DAHCs having electron-accepting core units and electron-donating substituents, as shown in Figure 1. We studied the carrier transport characteristics of DAHCs, CBP, and 1,3,5-tri(*N*-carbazolyl)-benzene (TCB) by observing their EL spectral characteristics. For different device structures, we observed systematic EL spectral changes, which reflected carrier injection and transport behavior changes in the DAHC layers.

II. Experimental Section

Absorption and photoluminescence (PL) spectra of DAHC-deposited films were measured using a UV−vis absorption spectrometer (UV-2550, Shimadzu Co.) and a fluorescence spectrometer (FP-6500-A-ST, Jasco Co.). Absolute PL quantum efficiency was measured with an integrating sphere (C9920-02, Hamamatsu Photonics Co.) with an Xe lamp ($\lambda_{max} = 337$ nm) as an excitation

(21) Aminaka, E.; Tsutsui, T.; Saito, S. *Jpn. J. Appl. Phys.* **1994**, *33*, 1061.
(22) Baldo, M. A.; Lamansky, S.; Burrows, P. E. *Appl. Phys. Lett.* **1999**, *75*, 4.
(23) Tsutsui, T.; Yang, M. J.; Yahiro, M.; Nakamura, K.; Watanabe, T.; Tsuji, T.; Fukuda, Y.; Wakimoto, T.; Miyaguchi, S. *Jpn. J. Appl. Phys.* **1999**, *38*, L1502.
(24) Adachi, C.; Kwong, R. C.; Djurovich, P.; Adamovich, V.; Baldo, M. A.; Thompson, M. E.; Forrest, S. R. *Appl. Phys. Lett.* **2001**, *79*, 2082.
(25) Inomata, H.; Goushi, K.; Masuko, T.; Konno, T.; Imai, T.; Sasabe, H.; Brown, J. J.; Adachi, C. *Chem. Mater.* **2004**, *16*, 1285.
(26) Chu, T. Y.; Ho, M. H.; Chen, J. F.; Chen, C. H. *Chem. Phys. Lett.* **2005**, *415*, 137.
(27) Son, K. S.; Yahiro, M.; Imai, T.; Yoshizaki, H.; Adachi, C. *J. Photopolym. Sci. Technol.* **2007**, *20*, 47.
(28) Son, K. S.; Yahiro, M.; Imai, T.; Yoshizaki, H.; Adachi, C. *Digest of Technical Papers of 7th IMID* **2007**, *7*, 1474.

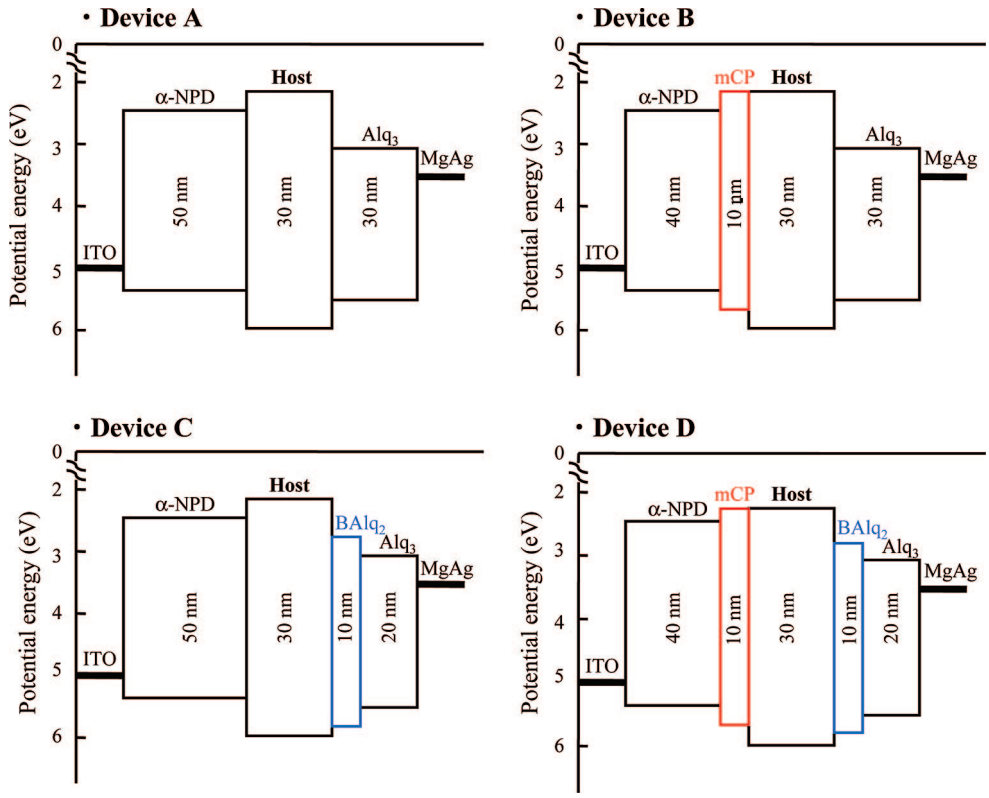

Figure 2. Device structures of Devices A, B, C, and D with HOMO−LUMO levels and work function of ITO and MgAg electrodes.

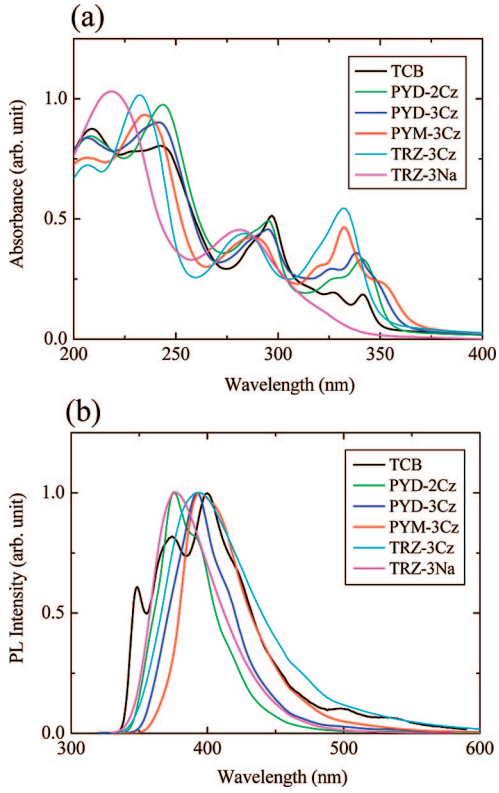

Figure 3. (a) Absorption and (b) PL spectra of 50-nm-thick DAHC thin films.

source.[29] For the optical measurements, 50-nm-thick DAHC films were deposited by high-vacuum (~1.0 × 10^{-3} Pa) thermal evaporation onto precleaned quartz substrates with a deposition rate of 0.3 nm/s. The highest occupied molecule orbital (HOMO) levels of the DAHC films were measured by UPS (AC-1, Riken Keiki Co.). The optical energy gaps (E_g) were estimated from the edge of the absorption spectra, and the lowest unoccupied molecule orbital (LUMO) levels were calculated by subtracting the E_g values from their HOMO levels. OLEDs were fabricated using the following steps. Organic layers and metal electrodes were deposited by high-vacuum (~1.0 × 10^{-3} Pa) thermal evaporation onto precleaned ITO-coated glass substrates, which had been degreased with solvents and cleaned in a UV-ozone chamber for 20 min. We fabricated four kinds of OLEDs, as shown in Figure 2. In Device A, 50-nm-thick α-NPD as a hole transport layer (HTL), 30-nm-thick DAHC layer as an emitting layer (EML), and 30-nm-thick Alq_3 as an electron transport layer (ETL) were formed. In Device B, an additional 10-nm-thick HTL of *N*,*N*′-dicarbazolyl-3,5-benzene (mCP) was inserted between the α-NPD and the DAHC layers in Device A. In Device C, an additional 10-nm-thick ETL of aluminum(III)-bis[2-methyl-8-quinolinate]4-phenylphenolate ($BAlq_2$) was inserted between the DAHC and the Alq_3 layers in Device A. In Device D, both 10-nm-thick mCP and $BAlq_2$ layers were inserted in Device A. In all devices, a cathode MgAg layer with the weight ratio of 10:1 and a 10-nm-thick Ag capping layer were deposited through a 1-mm-diameter opening in a shadow mask. EL spectra were obtained using a multichannel spectrometer (SD2000, Ocean Optics Inc.).

III. Results and Discussion

Figure 1 shows the chemical structures of (a) host materials, (b) the hole transport materials of α-NPD and mCP, and (c) the electron transport materials of Alq_3 and $BAlq_2$. The TCB is composed of three electron-donating carbazole substituents with a benzene core unit. The 2,4,6-tricarbazolo-1,3,5-pyridine (PYD-3Cz), PYM-3Cz, and TRZ-

(29) Kawamura, Y.; Sasabe, H.; Adachi, C. *Jpn. J. Appl. Phys.* **2004**, *43*, 7729.

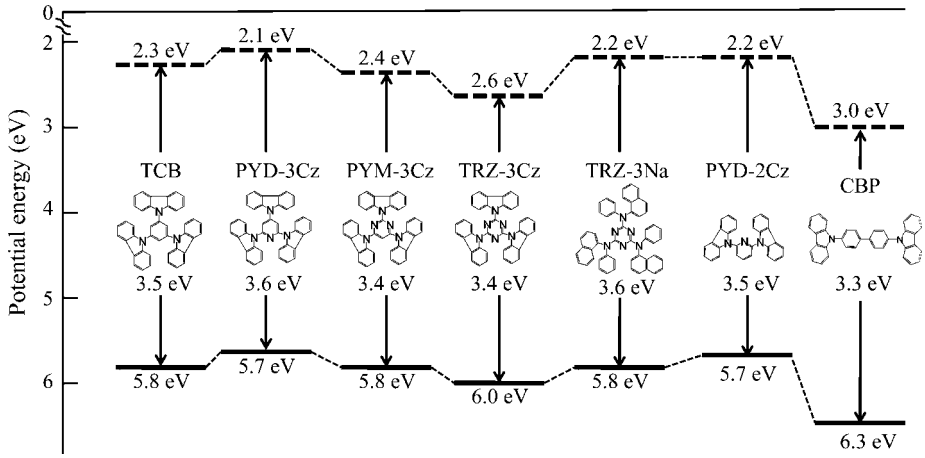

Figure 4. HOMO and LUMO levels of DAHCs, TCB, and CBP.

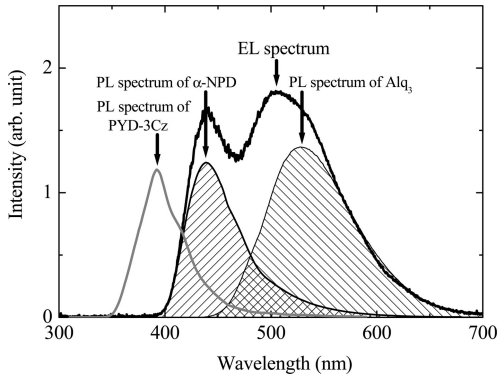

Figure 5. EL spectrum in Device A with PYD-3Cz as host at $J = 10$ mA/cm^2, resolved into PL components of α-NPD and Alq_3. PL spectrum of PYD-3Cz is also included.

3Cz also have the same electron-donating carbazole substituents respectively in different core units: pyridine in PYD-3Cz, pyrimidine in PYM-3Cz, and triazine in TRZ-3Cz. The TRZ-3Na is composed of three electron-donating substituents of β-naphthylamine attached to a triazine core unit. In addition, PYD-2Cz is composed of two electron-donating carbazole substituents with a pyridine core unit. Using these materials as a host layer, we estimated carrier transport characteristics. Figure 3 is a summary of (a) absorption and (b) the PL spectra of the DAHC deposited films. All DAHC films showed an onset of absorption around 350 nm and PL peaks around 400 nm at the short wavelength region, which indicated the presence of a wide energy gap.

Figure 4 shows the HOMO and LUMO energy levels of DAHCs, TCB, and CBP layers. First, we will describe the correlation between the molecular structures and energy levels. For PYD-3Cz, PYM-3Cz, and TRZ-3Cz the HOMO levels were 5.7, 5.8, and 6.0 eV and the LUMO levels were 2.1, 2.4, and 2.6 eV, respectively. These values show that the HOMO and LUMO levels of DAHCs layers shift to a deeper energy level with an increasing number of nitrogen atoms in the core units while their energy gaps are nearly independent of the core units. These experimentally obtained results show good agreement with the theorical calculation of energy levels in these heterocyclic compounds by Nenner and Schulz.[30] Furthermore, the TCB energy level is nearly identical to that of PYM-3Cz, and no systematic correlation with the HOMO and LUMO levels of PYD-3Cz, PYM-3Cz, and TRZ-3Cz was observed. This is probably due to the steric hindrance effect between the hydrogens in the benzene and three carbazole substituents in TCB. In addition, the energy levels of PYD-2Cz and PYD-3Cz are almost identical, indicating that the number of carbazole substituents has little influence on their energy levels. On the other hand, the HOMO and LUMO levels of TRZ-3Na were 0.2- and 0.4-eV shallower than those of TRZ-3Cz, indicating that the introduction of β-naphthylamine makes the HOMO and LUMO levels significantly shallower. These experimental results are in good agreement with the theoretical calculation by Chu et al.[26]

To understand practical carrier transport characteristics of DAHC layers in OLEDs, we prepared four kinds of OLED structures, as shown in Figure 2. By comparing EL spectra in these devices, we estimated the carrier transport characteristics of the DAHC host layers having different carrier injection barriers at their adjacent interfaces. When the EL spectrum is composed of only α-NPD or mCP components, we can reasonably conclude that the DAHC layers have unipolar electron transport characteristics. On the other hand, when the EL spectrum is composed of only $BAlq_2$ or Alq_3, we can conclude that the DAHC layers have unipolar hole transport characteristics. Furthermore, when the EL spectrum is composed of an emitter layer component and both hole and electron transport layer components, we can conclude that the DAHC layers have bipolar carrier transport characteristics. The reason we compared Devices A, B, C, and D was to clarify how the charge injection barrier between the host layers influences the position of the carrier recombination site.

Figure 5 shows the EL spectrum in an ITO/α-NPD/PYD-3Cz/Alq_3/MgAg/Ag device and reflects the estimation method used to determine the exciton production ratio (EPR) in this study. First, we noticed that the EL spectrum contains no PL component of the PYD-3Cz host layer. Only the PL components of α-NPD and Alq_3 were observed, indicating a very low carrier recombination probability in the PYD-3Cz layer. We thus estimated the EPR by resolving the EL spectra into both the α-NPD and Alq_3 components. To obtain the correct EPR, the photon numbers in the EL spectra were

(30) Nenner, I.; Schulz, G. J. *J. Chem. Phys.* **1975**, *62*, 1747.

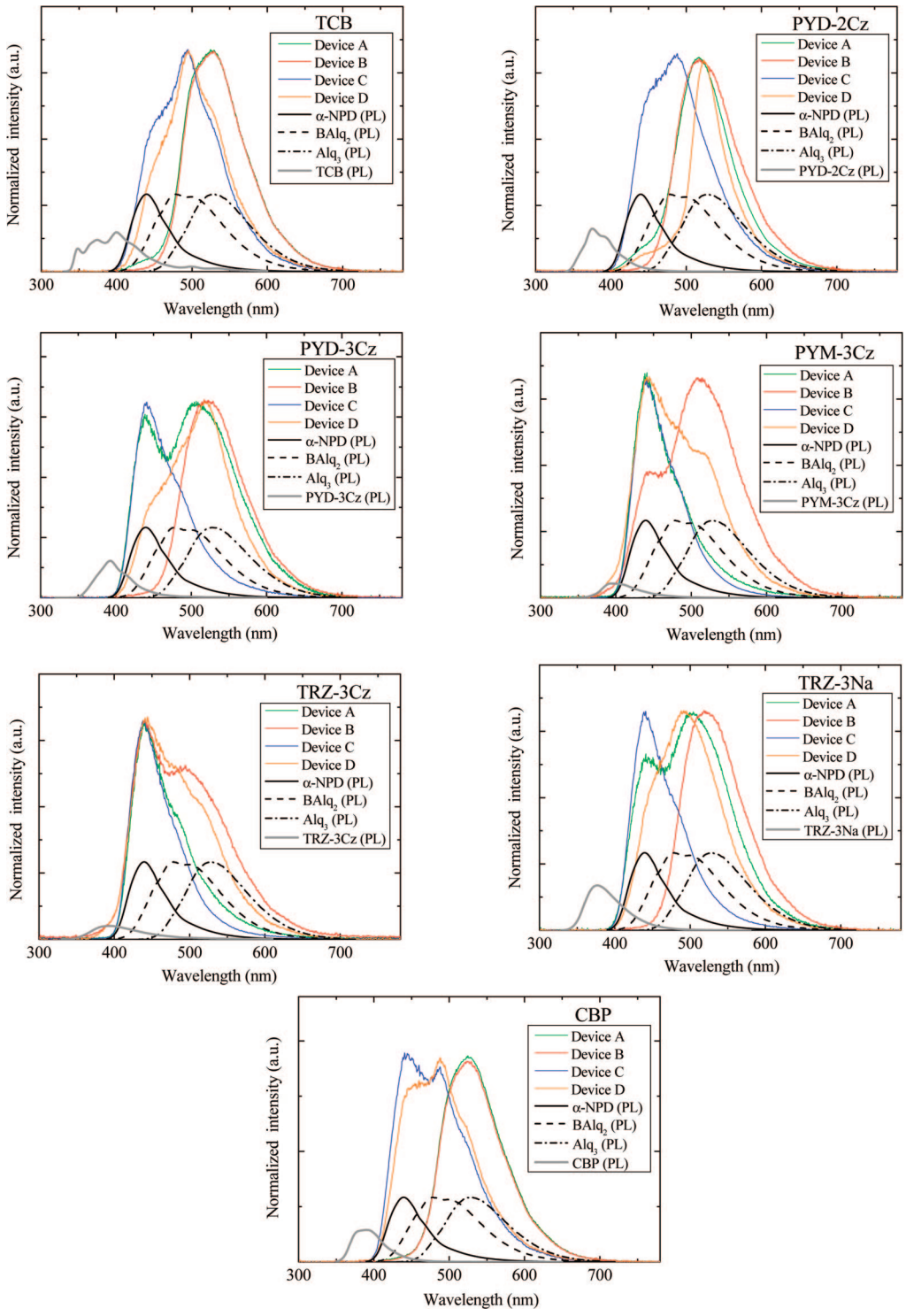

Figure 6. EL spectra of DAHCs in Device A, B, C, and D at $J = 10$ mA/cm^2 and PL spectra of α-NPD, $BAlq_2$, Alq_3, and each DAHC thin film.

converted to relative exciton numbers by dividing them by the absolute PL efficiencies (Φ_{PL}). To estimate the EPR in the α-NPD layer ($\eta_{\alpha\text{-NPD}}$), the relative EL intensity was divided by the PL efficiency of α-NPD ($\Phi_{PL} = 0.30$). In the same manner, the EPR in the Alq_3 layer was obtained by dividing the relative EL intensity by the PL efficiency of Alq_3 ($\Phi_{PL(Alq_3)} = 0.21$).

Figure 6 shows EL spectra in four device structures with seven different host layers along with the PL spectra of α-NPD-, $BAlq_2$-, and Alq_3-deposited films. In case of PYD-2Cz, for example, these EL spectra contained almost no PL components of DAHCs and mCP layers, and the spectra were mainly composed of α-NPD, $BAlq_2$, and Alq_3 emissions. Further, TCB, PYD-3Cz, TRZ-3Na, and CBP based devices showed similar emission characteristics. Here, we noticed that these EL spectra have a very low carrier recombination probability in the DAHC layers; almost all holes and electrons pass each other and move in opposite directions without carrier recombination. On the other hand, we noted that the EL spectra contained a low number of PL components of PYM-3Cz and TRZ-3Cz in Devices B and D. This is due to a significantly large electron injection barrier

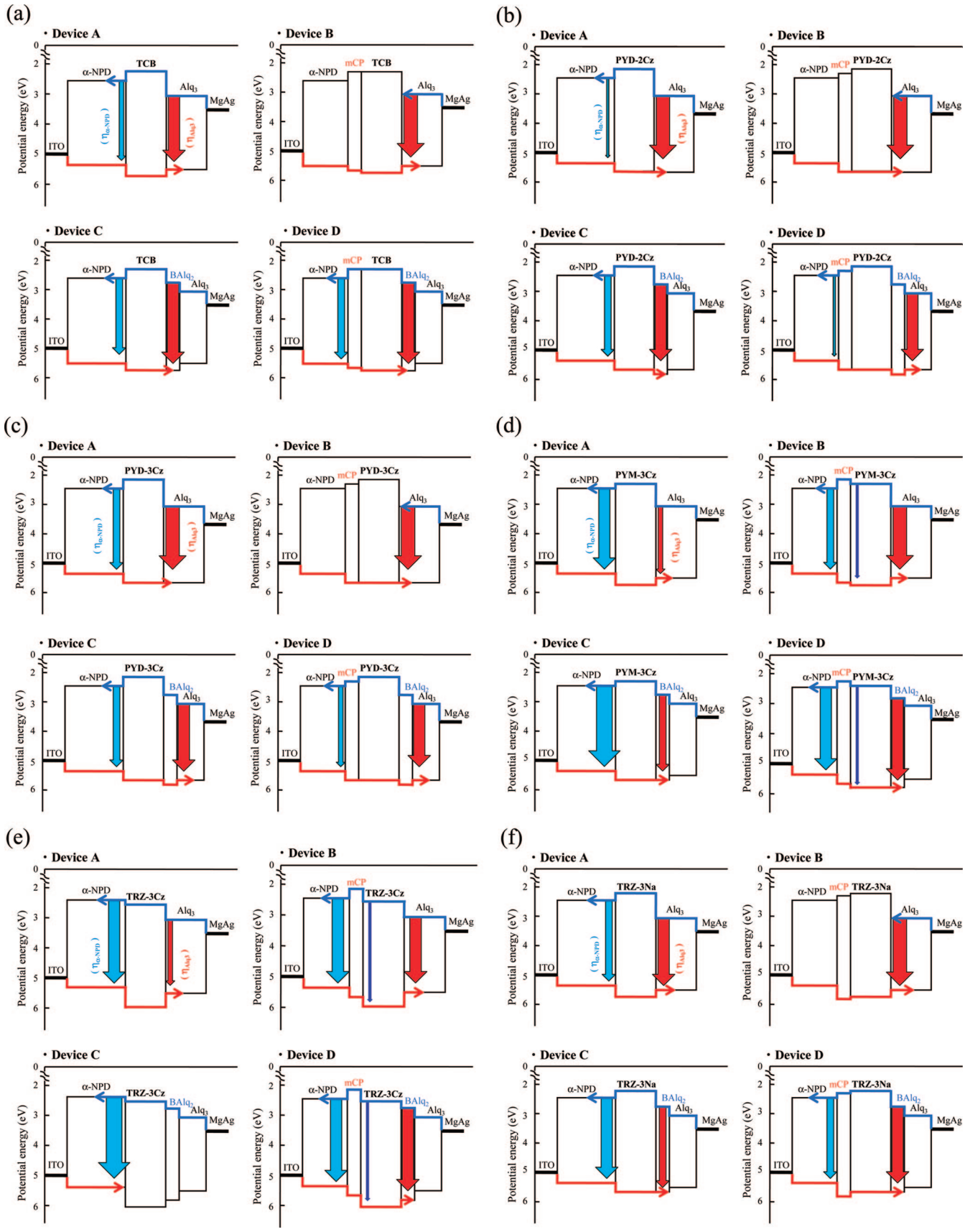

Figure 7. Schematic view of relative EL intensities depending on host layers and device configurations. Red and blue arrows respectively represent hole and electron flows in OLEDs.

between the DAHC and mCP heterointerfaces; the LUMO levels of PYM-3Cz (2.4 eV) and TRZ-3Cz (2.6 eV) are slightly deeper than that of mCP (2.3 eV), as shown schematically in Figure 7. This led to an accumulation of electrons and a successive carrier recombination with holes at these interfaces. These results indicate that DAHCs

Table 1. Exciton Production Ratio of DAHCs, TCB, and CBP in Various Device Structures (J = 10 mA/cm^2)

host layer	Device A $\eta_{\alpha\text{-NPD}}$:η_{Alq_3}	Device B $\eta_{\alpha\text{-NPD}}$:η_{Alq_3}	Device C $\eta_{\alpha\text{-NPD}}$:η_{BAlq_2}	Device D $\eta_{\alpha\text{-NPD}}$:η_{BAlq_2}
TCB	0.02:1.0	0:1.0	0.2:1.0	0.1:1.0
PYD-2Cz	0.05:1.0	0:1.0	0.4:1.0	0.05:1.0
PYD-3Cz	0.3:1.0	0:1.0	0.5:1.0	0.1:1.0
PYM-3Cz	2.3:1.0	0.3:1.0	7.7:1.0	0.8:1.0
TRZ-3Cz	2.3:1.0	1.0:1.0	1.0:0	0.9:1.0
TRZ-3Na	0.5:1.0	0:1.0	2.6:1.0	0.2:1.0
CBP	0:1.0	0:1.0	0.8:1.0	0.4:1.0

intrinsically have a very small carrier recombination cross-section (σ_{RE}) and the carrier recombination probability in the DAHC layers is enhanced by the introduction of the heterointerfaces. Such small σ_{RE} would be related to the peculiar electronic structures of DAHCs having both donor and acceptor moieties that individually contribute to hole and electron transport. Detailed analysis of σ_{RE} in relation with molecular electronic structures will be discussed in a separate paper.

Figure 7 shows a schematic view of carrier recombination in four devices with different host layers, and Table 1 and Figure 8 summarize the EPR numbers in all devices. First, we noticed that by changing the core unit from benzene (TCB) to pyridine (PYD), pyrimidine (PYM) and triazine (TRZ) tend to enhance electron current intensity, which is consistent with the electron-accepting nature of the core units. On the other hand, enhancement of hole current intensity was observed by changing the carbazole substituent into β-naphthylamine. In addition, comparing hole and electron current ratios in the PYD-2Cz and PYD-3Cz having the same pyridine core unit with different numbers of carbazole substituents, no substantial changes in the carrier transport characteristics were observed between them. From these results, we note that the most balanced bipolar characteristics were obtained with PYM-3Cz and TRZ-3Cz cores in Device A, B, and D.

We next discuss carrier balance characteristics for the device structures shown in Figure 8. In general, using a 10-nm-thick mCP layer (Device B) reduced the EPR of α-NPD, compared with Device A in which there was no EPR reduction. This indicates that the hole current is enhanced since no α-NPD emission was observed in these EMLs. However, by introducing a 10-nm-thick $BAlq_2$ layer (Device C), the EPR of α-NPD was significantly increased, indicating an increase of the electron current. In addition, by introducing both $BAlq_2$ and mCP (Device D), all devices showed bipolar characteristics. The most balanced bipolar condition of TCB, PYD-2Cz, PYD-3Cz, and CBP was obtained in Device C, indicating the cores of benzene, pyridine, and biphenyl with carbazole substituents have significantly stronger hole transport characteristics compared with electrons. Thus, the balanced bipolar condition was a result of the $BAlq_2$ layer, which reduces the electron injection barrier. On the other hand, PYM-3Cz and TRZ-3Cz showed a rather good bipolar condition in Devices B and D, indicating the core units of pyrimidine and triazine with carbazole substituents have strong electron transport characteristics. Thus, by introducing an mCP layer, reduction of the hole injection barrier resulted in a balanced current ratio. These results demonstrate that

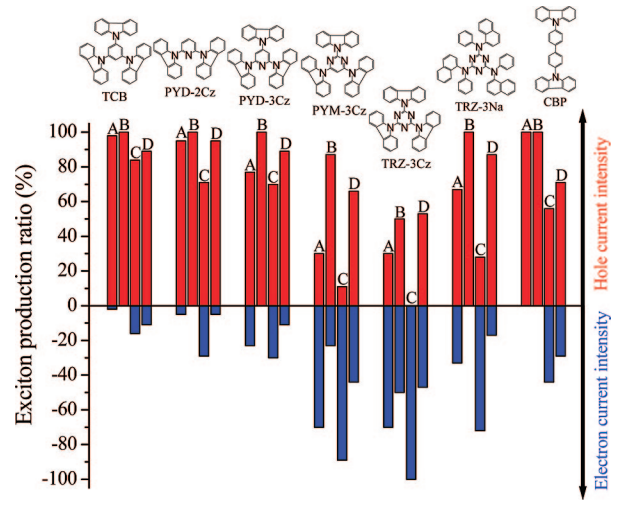

Figure 8. Relative hole and electron current intensities depending on four kinds of OLEDs.

charge injection and transport is delicately influenced by the insertion of HTL and ETL having different HOMO and LUMO energy levels. In organic semiconductors with no intentional doping of electron donors and acceptors, the carrier balance factor is affected not only by single electrical characteristics, such as carrier mobilities but also by carrier injection barriers between adjacent heterointerfaces. We could clearly observe that the hole and electron current ratio can be effectively controlled by changing molecular and device structures.

Finally we note weakness of our discussion. In our device configuration, Förster type energy transfer from TRZ-3Cz to Alq_3 and BAlq is basically possible. Thus, it may be possible that the emission spectra contain the contribution based on the energy transfer from the host layers to the adjacent carrier transport layers. In our present analysis, however, it is difficult to estimate the contribution of such energy transfer. In future study, it may be useful for applying the local doping method to understand the accurate carrier recombination and exciton formation regions.[31] Further, we tried to measure the motilities of the host layers by TOF method. However, the observed signals were basically dispersion type, resulted in difficulty for determining accurate carrier mobilities.

IV. Conclusion

We clarified carrier injection and transport characteristics of DAHCs by analyzing the EL spectra in various device structures. By changing the core units and substituent groups in DAHCs, the HOMO and LUMO levels are systematically controlled. Electron acceptor characteristics were strengthened by increasing the number of nitrogen atoms in the core unit. On the other hand, by changing carbazole into β-naphthylamine, hole injection and transport characteristics were strengthened. In addition to the donor and acceptor design of DAHCs, we could systematically control the carrier balance factor by design-

(31) Murata, H.; Merritt, C. D.; Kafafi, Z. H. *IEEE J. Sel. Top. Quantum Electron.* **1998**, *4*, 119.

ing a carrier injection barrier at heterointerfaces. In particular, PYM-3Cz and TRZ-3Cz showed the most balanced bipolar characteristics in these materials. Diarylamino-substituted heterocyclic compounds will be a useful host materials in terms of having well-balanced bipolar characteristics in phosphorescence OLEDs.

Acknowledgment. The present work is supported by a Grant-in-Aid for the Global COE Program, "Science for Future Molecular Systems" from the Ministry of Education, Culture, Science, Sports and Technology of Japan.

CM8004985